Automatic classification of serrated patterns in direct immunofluorescence images

Chenyu Shi[1], Joost M. Meijer[3], Jiapan Guo[1], George Azzopardi[1,2], Marcel F. Jonkman[3] and Nicolai Petkov[1]

[1]Johann Bernoulli Institute for Mathematics and Computer Science, University of Groningen, The Netherlands

[2]Intelligent Computer Systems, University of Malta, Malta

[3]Dermatology for Medical Sciences, University Medical Center Groningen (UMCG), University of Groningen, The Netherlands

Abstract: Direct immunofluorescence (DIF) images are used by clinical experts for the diagnosis of autoimmune blistering diseases. The analysis of serration patterns in DIF images concerns two types of patterns, namely *n*- and *u*-serrated. Manual analysis is time-consuming and challenging due to noise. We propose an algorithm for the automatic classification of serrated patterns in DIF images. We first segment the epidermal basement membrane zone (BMZ) where *n*- and *u*-serrated patterns are typically found. Then, we apply a bank of *B*-COSFIRE filters to detect ridges and determine their orientations with respect to the BMZ. Finally, we classify an image by comparing its normalized histogram of relative orientations with those of the training images using a nearest neighbor approach. We achieve a recognition rate of 84.4% on a UMCG data set of 416 DIF images, which is comparable to 83.4% by clinical experts.

1 Introduction

Manual analysis of serration patterns in direct immunouorescence (DIF) images is used by clinical experts for the diagnosis of certain skin diseases [5, 12–14]. One such disease is epidermolysis bullosa acquisita (EBA) [15], which is a chronic subepidermal blistering disease of the skin and mucus membranes. The serration pattern analysis concerns two types of patterns, which are referred to as *n*- and *u*-serrated, along the epidermal basement membrane zone (BMZ). The *n*-serrated patterns, an example of which is shown in Fig. 1a, are characterized

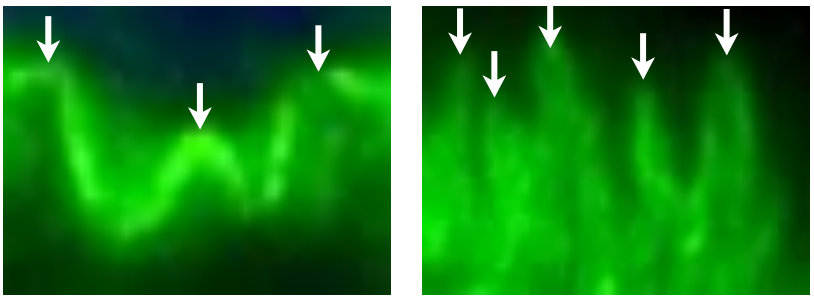

(a) (b)

Fig. 1: Examples of (a) *n*-serrated and (b) *u*-serrated patterns.

by undulating *n*-shapes. On the other hand, the *u*-serrated patterns comprise finger-like shapes, as shown in Fig. 1b. The manual analysis of serration patterns is very challenging mainly due to noise and lack of well-trained clinical experts and immunofluorescence microscopists [7, 12].

We propose an improvement of the method that we proposed in [11] for the classification of *n*- and *u*-serrated patterns. That method uses as a feature vector a histogram of absolute orientations of ridges. It does not consider the local orientation of the BMZ. Here, we first segment the BMZ and then we compute its local orientations. Subsequently, we apply a bank of *B*-COSFIRE filters [3] to detect ridges and determine their relative orientations with respect to the BMZ. Finally, we classify a test image by comparing its normalized histogram of relative orientations with those of the training images using a nearest neighbor approach.

The rest of the paper is organized as follows. In Section 2 we explain the proposed method. We evaluate it and report experimental results in Section 3. In Section 4, we draw conclusions.

2 Proposed method

2.1 Overview

In the following, we explain the main idea of the proposed method and subsequently we provide a detailed description of each step.

Fig. 2(a-f) show six examples of RGB DIF images. Fig. 2(a-c) and Fig. 2(d-f) contain *n*-serrated and *u*-serrated patterns, respectively. The dashed red lines enclose the BMZ. This is the area where *n*- or *u*-serrated patterns are located. For each DIF image, we first segment the BMZ by applying the preprocessing

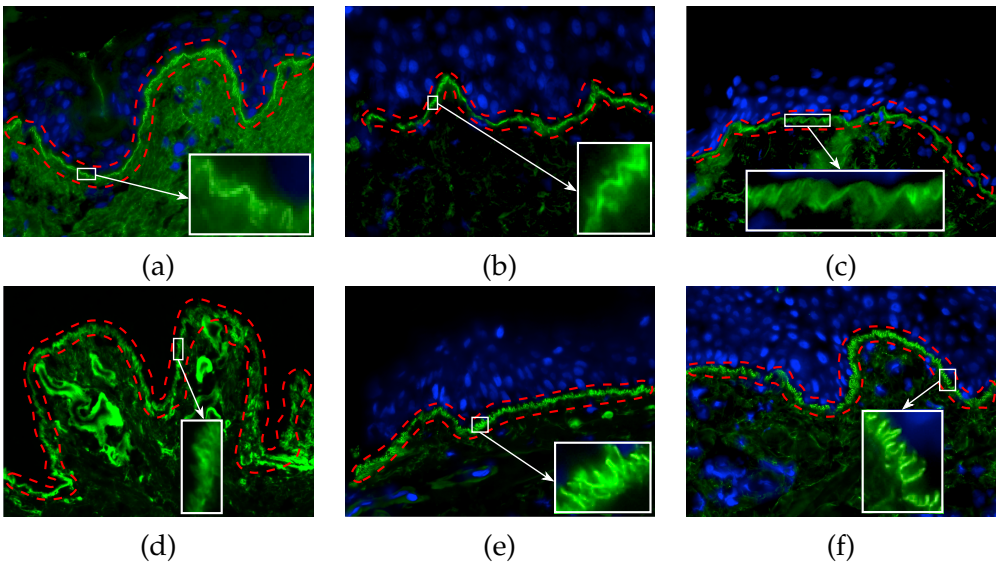

Fig. 2: Examples of RGB DIF images that contain (a-c) *n*-serrated and (d-f) *u*-serrated patterns. The red dashed lines indicate the BMZ.

algorithm, which we proposed in [11], to the green channel of the DIF image. Then, we compute the local orientation for each location along the BMZ by considering a small and a large neighbourhood, respectively. For the small neighbourhood we use *B*-COSFIRE ridge detectors and for the larger neighbourhood we use the orientation measurement approach introduced in [4]. The former measurement gives the absolute orientations of the serrated pattern, while the latter measurement determines the orientation of the baseline. Finally, we compute the relative orientations and represent every DIF image by a normalized histogram of such orientations.

2.2 Segmentation of the BMZ

We use the algorithm that we proposed in [11] to segment the BMZ from the green channel of a DIF image (of size 1392×1040 pixels), Fig. 3b. First, we use a disk-shaped structuring element (radius of 30 pixels) to perform morphological closing followed by a flood-fill operation, of which the result is shown in Fig. 3c. Then, we use Canny edge detector [6] to extract the upper-most boundary of the largest connected component. In order to avoid the border effect, we remove 50 pixels from each side of the image. Fig. 3d shows the extracted boundary. We obtain the BMZ mask (Fig. 3e) by dilating the extracted boundary using a disk-shaped structuring element (radius of 30 pixels). Finally, we use the resulting BMZ mask to extract the corresponding region of the green channel of a DIF image (Fig. 3f).

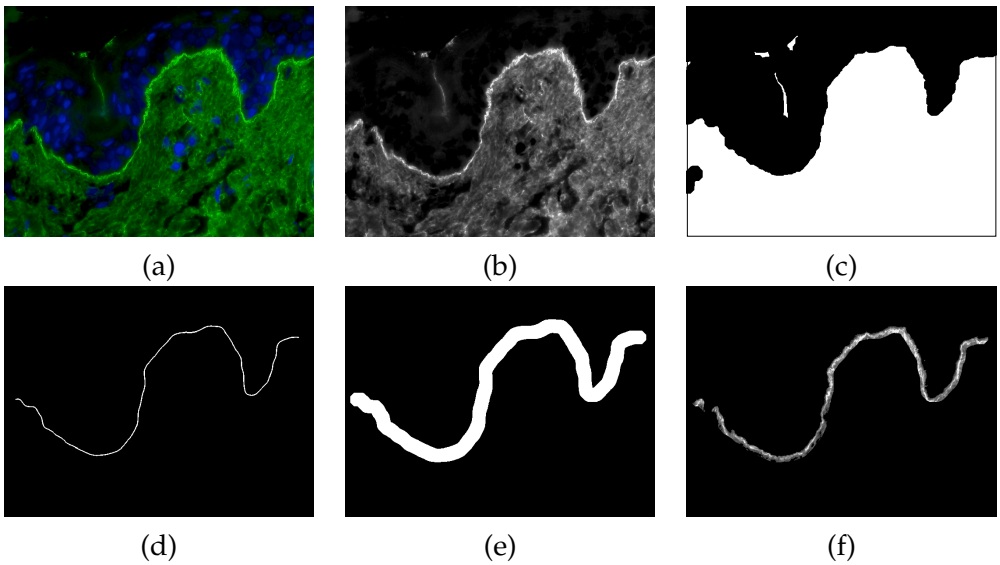

Fig. 3: (a) An example of a RGB DIF image (of size 1392×1040 pixels) and (b) its green channel image. (c) The resulting binary image of a morphological closing operation using a disk-shaped structuring element (radius of 30 pixels) applied to the green channel image. (d) The extracted boundary between the dark and white regions of the binary image. (e) Binary mask of the BMZ and (f) the product of the green channel image and the mask.

2.3 Determination of the local BMZ orientation

We compute the local BMZ orientation $\phi(x, y)$ at a given location (x, y) by an orientation measurement approach introduced in [4]. Fig. 4 illustrates this method. For a point A on the BMZ mask (Fig. 3e), we consider the intensity pixels of the corresponding boundary map (Fig. 3d) along a circle of a given radius $r = 50$ pixels. Two positions (B and C) are chosen as the points that characterize the local orientations. We determine the angles of the polar coordinates for such points with respect to the point A. For instance, the leg from B to A forms an inbound angle $\phi_1 = 0.72$ radians, and the leg from A to C forms an outbound angle $\phi_2 = 3.40$ radians. Then we compute the local orientation $\phi(x, y)$ of A with respect to B and C as:

$$\phi(x, y) = ||\pi/2 - (\phi_1 + \phi_2)/2||_\pi \tag{1}$$

where $||\cdot||_\pi$ represents the modulus of π. For this example, $\phi(A) = 0.49$ radians.

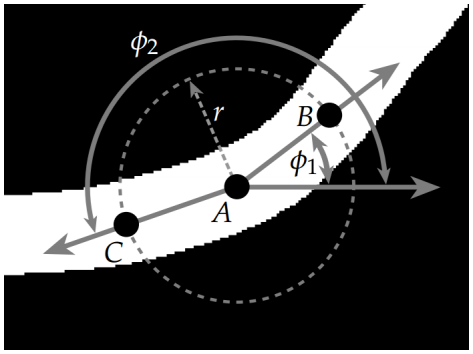

Fig. 4: Part of a BMZ mask from Fig. 3e.

2.4 Determination of ridge orientation

We use *B*-COSFIRE filters[1] [3] to detect ridges and determine their orientations. A *B*-COSFIRE filter is a ridge detector, which is based on the COSFIRE approach [2] and the CORF computational model [1]. Its response is achieved by computing the geometric mean of a group of linearly aligned responses of a Difference-of-Gaussians (DoG) filter. A *B*-COSFIRE filter has three main parameters: the standard deviation σ of the outer Gaussian function in the involved DoG filter[2], the radius l and the orientation θ. Further to the experiments we did in [11], we use $\sigma = 1.2$ and $l = 4$. Here, we only mention that we use 16 *B*-COSFIRE filters with $\theta \in (0, \pi/16, \ldots, 15\pi/16)$. Fig. 5a shows an example of a *B*-COSFIRE filter that is selective for ridges with an orientation $\theta = \pi/6$ radians and Fig. 5c shows its response map to the input image shown in Fig. 5b. These filters have other parameters which we skip here for brevity. We refer the interested reader to [1–3, 8–11] and to an online implementation[3].

For each BMZ, we apply a bank of 16 *B*-COSFIRE filters that are selective for different orientations. We denote by $\Theta(x, y)$ the local orientation of a ridge point as:

$$\Theta(x, y) = ||\pi/2 + \theta(x, y)||_\pi \tag{2}$$

where $\theta(x, y)$ represents the orientation of the *B*-COSFIRE filter that exhibits the maximum response at the location (x, y).

[1]Matlab scripts: `http://www.mathworks.com/matlabcentral/fileexchange/49172`
[2]The standard deviation of the inner Gaussian function is 0.5σ
[3]`http://matlabserver.cs.rug.nl`

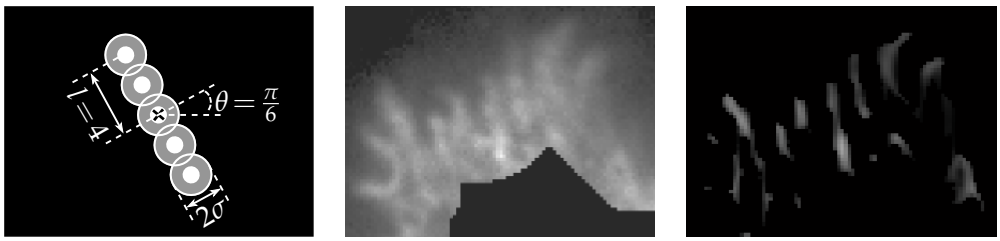

(a) (b) (c)

Fig. 5: (a) Structure of a *B*-COSFIRE filter which is used for detecting the ridges with an orientation $\theta = \pi/6$ radians. The cross marker indicates the support center of the filter. The radius l indicates the farthest distance from the center of the filter that takes as inputs five responses from a center-on DoG filter with $\sigma = 1.2$. The locations of the afferent inputs are equally spaced in intervals of 2 pixels. (b) A cropped region of a DIF image and (c) the corresponding *B*-COSFIRE response map.

2.5 Descriptor: normalized histogram of relative orientations

We denote by $\Phi(x,y)$ the relative orientation of a ridge at position (x,y) with respect to the BMZ orientation $\phi(x,y)$:

$$\Phi(x,y) = \begin{cases} \pi - ||\phi(x,y) - \Theta(x,y)||_\pi, & \text{if } ||\phi(x,y) - \Theta(x,y)||_\pi > \pi/2 \\ ||\phi(x,y) - \Theta(x,y)||_\pi, & \text{otherwise} \end{cases} \quad (3)$$

In this way, we obtain a map of the relative orientations for the BMZ of each DIF image. We construct the L1-normalized histogram of these orientations and use it as the feature vector of a DIF image. Fig. 6(a-f) show the normalized histograms of the images in Fig. 2.

3 Evaluation

3.1 Data set

We use a data set provided by the University Medical Center Groningen (UMCG). It comprises 26 DIF images from different pemphigoid patients, 15 of which contain *n*-serrated patterns and the rest contain *u*-serrated ones. We expand the data set to 416 DIF images by rotating each of the 26 images from $\pi/8$ to 2π radians in intervals of $\pi/8$ radians. All images are taken with magnifications of $\times 40$, which is the most commonly used scale in hospitals. The data set is publicly available as an online test[4].

[4] `http://www.nversusu.umcg.nl/`

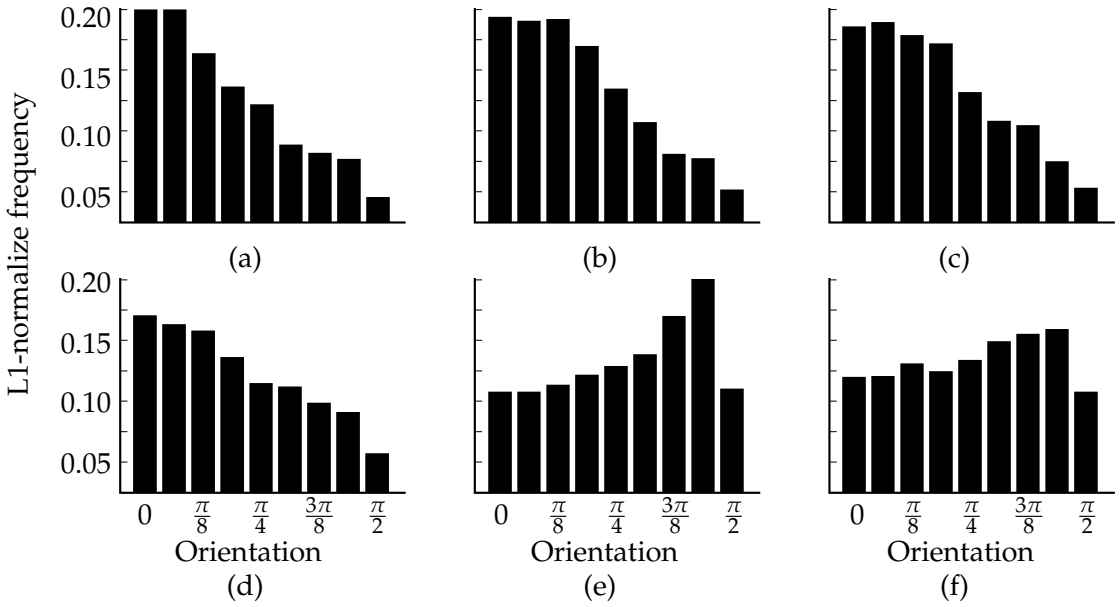

Fig. 6: (a-f) Six L1-normalized histograms of the relative orientations of the DIF images in Fig. 2(a-f), respectively.

3.2 Experiments

We apply the proposed method to all 416 DIF images of the UMCG data set and for every DIF image we compute the L1-normalized histogram of the relative orientations. For the evaluation of the proposed method, we use the nearest neighbor algorithm to classify each image as u-serrated or n-serrated by comparing its histogram with the ones of the remaining DIF images in the data set. In Table 1, we report the results that we obtain for different similarity measures between the histograms. By using leave-one-out cross-validation, we achieve a recognition rate of 84.4% on the expanded UMCG data set.

Table 1: Recognition rates achieved for different distance measures.

	Chi-square	Euclidean	Cosine	Correlation	Cityblock
Method in [11]	**69.9%**	69.0%	63.0%	63.7%	65.6%
Proposed method	**84.4%**	84.4%	75.5%	73.3%	83.4%

4 Conclusions

We achieve the recognition rate of 84.4% on the expended UMCG data set of 416 DIF images, which is significantly better than the 69.9% that we achieve by the previous method [11] and that it is comparable to the 83.4% achieved by clinical experts [12].

References

[1] Azzopardi, G., Petkov, N.: A CORF computational model of a simple cell that relies on LGN input outperforms the Gabor function model. Biological Cybernetics 106(3), 177–189 (2012)

[2] Azzopardi, G., Petkov, N.: Trainable COSFIRE filters for keypoint detection and pattern recognition. IEEE Transactions on Pattern Analysis and Machine Intelligence 35(2), 490–503 (2013)

[3] Azzopardi, G., Strisciuglio, N., Vento, M., Petkov, N.: Trainable COSFIRE filters for vessel delineation with application to retinal images. Medical Image Analysis 19(1), 46–57 (2015)

[4] Brinka, A., Smitb, J., Bulacua, M., Schomakera, L.: Writer identification using directional ink-trace width measurements. Pattern Recognition 45(1), 162–171 (2012)

[5] Buijsrogge, J.J.A., Diercks, G.F.H., Pas, H.H., Jonkman, M.F.: The many faces of epidermolysis bullosa acquisita after serration pattern analysis by direct immunofluorescence microscopy. British Journal of Dermatology 165(1), 92–98 (2011)

[6] Canny, J.: A computational approach to edge detection. IEEE Transactions on Pattern Analysis and Machine Intelligence 8(6), 679–698 (1986)

[7] Gammon, W., Kowalewski, C., Chorzelski, T., Kumar, V., Briggaman, R., Beutner, E.: Direct immunofluorescence studies of sodium chloride-separated skin in the differential diagnosis of bullous pemphigoid and epidermolysis bullosa acquisita. Journal of the American Academy of Dermatology 22(4), 664–670 (1990)

[8] Petkov, N.: Biologically motivated computationally intensive approaches to image pattern-recognition. Future Generation Computer Systems 11(4-5), 451–465 (1995)

[9] Petkov, N., Kruizinga, P.: Computational models of visual neurons specialised in the detection of periodic and aperiodic oriented visual stimuli: Bar and grating cells. Biological Cybernetics 76(2), 83–96 (1997)

[10] Petkov, N., Westenberg, M.: Suppression of contour perception by band-limited noise and its relation to non-classical receptive field inhibition. Biological Cybernetics 88(10), 236–246 (2003)

[11] Shi, C., Guo, J., Azzopardi, G., Meijer, J.M., Jonkman, M.F., Petkov, N.: Automatic differentiation of u- and n-serrated patterns in direct immunofluorescence images. Computer Analysis of Images and Patterns (CAIP 2015), Lecture Notes in Computer Science 9256 (Springer), in print, (2015)

[12] Terra, J.B., Meijer, J.M., Jonkman, M.F., Diercks, G.F.H.: The n- vs. u-

serration is a learnable criterion to differentiate pemphigoid from epidermolysis bullosa acquisita in direct immunofluorescence serration pattern analysis. British Journal of Dermatology 169(1), 100–105(2013)

[13] Terra, J.B., Pas, H.H., Hertl, M., Dikkers, F.G., Kamminga, N., Jonkman, M.F.: Immunofluorescence serration pattern analysis as a diagnostic criterion in antilaminin-332 mucous membrane pemphigoid: immunopathological findings and clinical experience in 10 Dutch patients. British Journal of Dermatology 165(4), 815–822 (2011)

[14] Vodegel, R., Jonkman, M., Pas, H., De Jong, M.: U-serrated immunodeposition pattern differentiates type VII collagen targeting bullous diseases from other subepidermal bullous autoimmune diseases. British Journal of Dermatology 151(1), 112–118 (2004)

[15] Woodley, D.T., Briggaman, R.A., O'Keefe, E.J., Inman, A.O., Queen, L.L., Gammon, W.R.: Identification of the skin basement-membrane autoantigen in epidermolysis bullosa acquisita. New England Journal of Medicine 310(16), 1007–1013 (1984)